

Unravelling intrusion-induced forced fold kinematics and ground deformation using 3D seismic reflection data

Jennifer Reeves [†], Craig Magee ^{*†}, Christopher A-L. Jackson [†]

ABSTRACT

Sills emplaced at shallow-levels are commonly accommodated by overburden uplift, producing forced folds. We examine ancient forced folds developed above saucer-shaped sills using 3D seismic reflection data from the Canterbury Basin, offshore SE New Zealand. Seismic-stratigraphic relationships indicate sill emplacement occurred incrementally over ~31 Myr between the Oligocene (~35–32 Ma) and Early Pliocene (~5–4 Ma). Two folds display flat-topped geometries and amplitudes that decrease upwards, conforming to expected models of forced fold growth. Conversely, two folds display amplitudes that locally increase upwards, coincident with a transition from flat-topped to dome-shaped morphologies and an across-fold thickening of strata. We suggest these discrepancies between observed and expected forced fold geometry reflect uplift and subsidence cycles driven by sill inflation and deflation. Unravelling these forced fold kinematic histories shows complex intrusion geometries can produce relatively simple ground deformation patterns, where magma transgression corresponds to localisation of uplift.

1 INTRODUCTION

Uplift of Earth's surface in response to shallow-level magma movement provides crucial insights into volcano activity, potentially warning of impending eruptions (e.g., Sturkell et al., 2006; Biggs et al., 2009; Sparks et al., 2012; van Wyk de Vries et al., 2014). Inverting ground deformation patterns recorded at monitored volcanoes to map magma movement is difficult, however, because we cannot directly observe the host rock deformation mechanisms accommodating intrusion or validate models (Galland, 2012). We thus typically assume that ground deformation results from elastic bending of the overburden (i.e. forced folding), such that the area of surface uplift is expected to directly correlate to the location and size of an underlying intrusion (Galland, 2012). Importantly, analyses of forced folds above sills and laccoliths exposed at Earth's surface, generated in analogue models, modelled analytically, or imaged in seismic reflection data reveal that a combination of elastic bending and inelastic processes (e.g. faulting, fluidisation, and pore collapse) can accommodate magma emplacement (e.g., Pollard and Johnson, 1973; Johnson, 1987; Galland and Scheibert, 2013; Jackson et al., 2013; Magee et al., 2013; van Wyk de Vries et al., 2014; Montanari et al., 2017). The likely occurrence of inelastic deformation processes implies that traditional inversion of ground deformation data assuming pure elastic bending of the host rock will underestimate magma

* Corresponding author: c.magee@imperial.ac.uk

[†] Basins Research Group, Imperial College London, London, SW7 2BP, UK

volumes (e.g., Schofield et al., 2014). It thus remains challenging to compare active and ancient systems because the dynamic deformation processes that cumulatively build a forced fold are difficult to deduce when magmatism has long-since ceased.

Here, we analyse a magma plumbing system imaged in 3D seismic reflection data from the petroliferous Canterbury Basin, offshore SE New Zealand (Fig. 1), and identify four saucer-shaped sills intruded into Cretaceous-to-Eocene strata. The sills are overlain by dome-shaped forced folds and generated hydrothermal vents above their lateral tips. Because intrusion-induced forced folds and hydrothermal vents are expressed as topographic or bathymetric highs at the contemporaneous surface, numerous studies have used the age of overlying strata that onto these structures as a method for determining the timing of magmatism (e.g., Trude et al., 2003; Jamtveit et al., 2004; Hansen and Cartwright, 2006; Magee et al., 2013). Whilst most studies assume that onlap of strata onto the top of forced folds marks the age of instantaneous emplacement (Trude et al., 2003), we show that multiple onlap events can be recognised throughout the folded sedimentary succession. Our analysis of seismic-stratigraphic relationships between the hydrothermal vents, forced folds, and overlying strata reveals three main phases of forced fold growth and thus sill emplacement in the Oligocene (~35–32 Ma), Miocene (~19–16 Ma), and Pliocene (~5–4 Ma); these phases of emplacement indicate magmatism overlapped with and may have impacted petroleum generation, migration, and accumulation. Seismic-stratigraphic onlap onto intrusion-induced forced folds is thus a powerful tool for determining timing of magmatic activity (e.g., Trude et al., 2003), although we demonstrate that we should not solely rely on defining strata onlapping onto the top of forced folds to constrain emplacement age (Magee et al., 2014). Identifying seismic-stratigraphic relationships throughout folded sequences allows forced fold kinematics to be unravelled and we show, for the first time, that intermittent subsidence can play an important role in intrusion-induced forced folding.

20

Figure 1: Location map of the study and available seismic reflection and borehole data used.

2 GEOLOGICAL SETTING

25 The Canterbury Basin, located offshore SE New Zealand (Fig. 1), is bound by the Chatham Rise to the north-east and the Bounty Trough to the south-east. Basin formation occurred in response to rifting between New Zealand, Antarctica, and Australia in the Late Albian-to-Early Campanian (Fig. 2) (e.g., Fulthorpe et al., 1996; Lu and Fulthorpe, 2004). The basement broadly corresponds to the Torlesse Supergroup, a series of Permian-to-Early Cretaceous greywacke and argillite meta-sedimentary rocks (Uruski, 2010). Graben and half-graben formed during the middle Cretaceous phase of rifting broadly strike E-W and were infilled by fluvial and paralic sediments, including coal that forms the main source rock in the region (Fig. 2) (i.e. the Horse Range and Katiki formations; Carter, 1988; Killops et al., 1997; Uruski, 2010; Ghisetti and Sibson, 2012). The onset of passive subsidence and a marine transgression in the Late Cretaceous defined the transition to the post-rift period, characterised stratigraphically by the upwards progression from terrestrial sandstone and coal (i.e. the Pukeiwhai Formation) to deposition of marine sandstone, mudstone, and siltstone (Fig. 2) (i.e. the Katiki, Moreaki, and Hampden formations; Carter,

30

1988; Killops et al., 1997). Some of the Paleogene mudstone represent potential source rocks (Fig. 2) (Bennett et al., 2000). Overlying these formations is the marine Amuri Limestone (Fig. 2) (Fulthorpe et al., 1996). The point of maximum transgression at ~29 Ma is marked in the Canterbury Basin by a regional unconformity (Fig. 2) (e.g., Carter, 1988; Fulthorpe et al., 1996). Continued uplift and an increase in the supply of terrigenous silt and sand drove the eastward progradation of continental shelf and slope deposits in the Early Miocene-to-Recent (Fig. 2) (i.e. the Tokama Siltstone; Lu et al., 2005). Hydrocarbon generation, migration, and accumulation in the Canterbury Basin likely began in the ~Middle Miocene when Middle-to-Late Cretaceous coals were buried to sufficient depths (Fig. 2) (e.g., Bennett et al., 2000). Most plays rely on stratigraphic traps within Upper Cretaceous sandstone reservoirs, although Eocene sandstone reservoirs within Miocene fault- and fold-related structural traps also form viable prospects (Fig. 2) (Bennett et al., 2000).

10

Figure 2: Tectono-stratigraphic framework of the Canterbury Basin highlighting ages of onshore magmatic events and phases of petroleum system development (after Carter, 1988; Fulthorpe et al., 1996; Killops et al., 1997; Bennett et al., 2000; Timm et al., 2010; Uruski, 2010). Magmatic events correspond to: A = Geraldine and Timaru Lavas; B = Banks Peninsula; C = Cookson Volcanics; and D = View Hill, Central Canterbury (Timm et al., 2010). Petroleum system elements correspond to: So = source rock; R = reservoir rock; Se = Seal; and G = hydrocarbon generation.

3 DATASET AND METHODOLOGY

We use a pre-stacked time-migrated (PSTM) 3D seismic reflection survey (Waka) tied to three regional boreholes (i.e. Galleon-1, Endeavour-1, and Cutter-1) by PSTM 2D seismic surveys (Fig. 1). The 3D seismic data cover a ~1428 km² area, of which we focus on ~314 km² (Fig. 1). Inline (NE–SW) and crossline (NW–SE) spacing is 25 m and 12.5 m, respectively. The data are displayed with a SEG normal polarity, whereby a downward increase in acoustic impedance corresponds to a positive (red) reflection. Within the focused study area, the water depth is 863–1948 ms TWTT (two-way travel time), or 647–1461 m assuming a water velocity of 1480 m s⁻¹. Three, NW-trending submarine canyons are developed at the seabed (Fig. 3A), with seismic reflections directly beneath them being down-warped, decreasing in amplitude with depth, and mirroring the channel plan-view morphology (Fig. 3B). We consider that the apparent expression of the submarine channels within the underlying reflections reflection is a geophysical artefact attributable to velocity push-down, caused by acoustically slow seawater being juxtaposed against shallowly buried, but still acoustically faster sediment/rock.

Figure 3: (A) Map of the seabed in the study area highlighting the presence of three, deep seafloor canyons. (B) Time-migrated and depth-converted seismic sections showing the effect of velocity push-downs related to the seafloor canyons and the four sills and forced folds studied. Depth-converted seismic sections with vertical exaggeration (VE), to better highlight the fold geometries, and without are shown for comparison. See Figures 1 and 3A for location.

We use borehole data to define the age and lithology of ten mapped stratigraphic horizons (H1-H10) (Figs 2 and 3); four sills (S1-S4) were also mapped (Fig. 3). All three wells display consistent time-depth relationships, suggesting that the area of interest has a simple velocity structure (Fig. 4). We use a 2nd order polynomial best-fit line to the checkshot data from the three boreholes to broadly define interval velocities for the Seabed–H10 (1800 m s⁻¹), H10–H2 (2800 m s⁻¹), and H2–H1 (3600 m s⁻¹). However, the boreholes are located on the continental shelf where stratigraphy is ~700 ms TWTT shallower and thinner than in the area covered by the 3D seismic survey (Fig. 1), implying that these velocities are probably minimum estimates for those encountered in our study area. We use our simple velocity model to depth convert structural maps and measurements from time to depth. Depth-conversion of the seismic data using the derived velocity was attempted in order to remove the velocity push-down artefacts, which hinder our geometric interpretation of the seismically imaged geology. Whilst we were unable to fully remove the imprint of the velocity push-downs, which suggests our simple model utilised does not fully capture the true velocity structure of the study area, the depth-conversion significantly reduced their imaging impact and, thereby, facilitated greater confidence in structural interpretations (Fig. 3B). Using our simple velocity model we created depth-structure and isopach maps for and between key stratigraphic horizons, respectively, thereby highlighting lateral variations in stratal thickness that may be related to tectonics and magmatism.

15

Figure 4: Two-way travel time versus depth curve for the Galleon-1, Cutter-1, and Endeavour-1 boreholes.

A dominant frequency that decreases downwards from ~35 Hz to 25 Hz within the interval of interest, coupled with the inferred velocity structure, suggests that the limit of separability within the data increases with depth from 13 m to 36 m; we calculate the limit of visibility to increase from 2 m to 5 m (Brown, 2004). Assuming an interval velocity of 5550 m s⁻¹ for the mapped intrusions (Skogly, 1998) and taking the local dominant frequency of ~25 Hz, we estimate that the limits of separability and visibility are 55 m and 7 m, respectively. Sills between 7–56 m thick will therefore be expressed in seismic data as tuned reflection packages, i.e. where reflections from the top and base intrusion contacts constructively interfere and cannot be distinguished, meaning we cannot calculate true sill thickness.

25

4 RESULTS

4.1 Sills

We mapped three, broadly saucer-shaped sills (S1–S3) and one strata-concordant sill (S4), which are expressed as packages of high-amplitude reflections (Figs 3 and 5-7). The saucer-shaped sills consist of a strata-concordant inner sill (partly encompassed by an inclined, transgressive limb (Figs 3 and 5-7). The base of S1 is located immediately below H2, although there is a south-dipping inclined sheet that extends from S1 down to the basement-cover interface (H1) (Figs 3, 6A, and C). The basal strata-concordant sections of S2–S4 typically coincide with H1 (Figs 3 and 7). S1 and S2 are elongated ENE-WSW

and ESE-WSW and their long axes and plan-view aspect ratios are 6.3 km and 7.5 km, and 1.5 and 1.7, respectively; the inner sill length of both S1 and S2 is 4.5 km (Fig. 5). In detail, S3 has an ESE-WSW oriented long axis and consists of several saucer-like depressions bound by transgressive inclined limbs, which become shallower towards the NE (Figs 5 and 7A). S4 occurs between S1 and S2, displays a rather irregular inner sill morphology, is roughly elongated ESE-WSW, and shallows to the NE (Fig. 5). S3 and S4 extend beyond the limits of the 3D seismic survey, thus we cannot determine their true dimension. However, their long axes are a minimum of 9.1 km (S3) and 14.5 km (S4) (Fig. 5).

Figure 5: Depth-structure map of S1–S4 highlighting the location of reverse faults around sill edges and the position folds 1–4.

10

Figure 6: Seismic sections and line interpretations through S1 and Fold 1. See Figure 5 for locations.

Figure 7: Seismic sections and line interpretations through S2 and Fold 2 (A), and S3 and Fold 3 (B). See Figure 5 for locations.

15 4.2 Supra-sill structure

The top of the basement (H1) in the study area is dominated by a NE-trending, ~29 km long, ~0.5 km high ridge along its south-eastern boundary, but also displays a series of smaller, variably shaped structural highs (Fig. 8). Overlying strata onlap the basement (H1) and dip gently eastward (Fig. 3B). Superimposed onto the regional structure of H2–H8 are three, prominent elliptical folds (i.e. folds 1–3) that have long axes of 6.2 km, 6.4 km, and 4.6 km respectively (Fig. 8). The true geometry of Fold 3 is difficult to ascertain because its south-eastern limit appears to coincide with an area of velocity push-downs related to seabed submarine canyons (Figs 3B and 8). A broad, 11 km long elliptical dome is also observed between H2–H8 (i.e. Fold 4; Fig. 8). The outlines of folds 1–2 overlie the lateral terminations of S1 and S2, respectively, Fold 3 overlies a relatively shallow portion of S3, and the central part of Fold 4 is underlain by S4 (Fig. 5).

25 Figure 8: Depth-structure maps for H1, H3, H5, H8, and H10.

4.2.1 Fold geometries between H2–H8

Between H2–H8, folds 1 and 2 have relatively flat-tops, parallel to the regional structural dip of the host sedimentary sequence, and are bound by monoclines (Figs 3 and 6–8). At lower stratigraphic levels (e.g. H3 and H5), the centre of Fold 1 appears to be depressed relative to its margins (Fig. 8). Low-throw (<50 m) reverse faults coincident with and extending up to H8 above the S1 inclined limbs, offset the Fold 1 monoclines around ~9 km of the ~14 km fold circumference (Figs 5 and 6). Above the inclined limbs of S2, three laterally restricted (~0.9–1.8 km long), low-throw (<50 m) reverse faults offset the Fold 2 monoclines within the H3–H7 sequence (Figs 3B and 5). The maximum amplitudes at H3 for the two folds are ~51 m (Fold

30

1) and ~54 m (Fold 2), whereas maximum amplitudes at H8 are 59 m (Fold 1) and 78 m (Fold 2) (Figs 6, 7A, and 8). Compared to folds 1 and 2, Fold 3 has a more rounded top and has a maximum amplitude of 110 m at H8 (Figs 7B and 8). The amplitude of Fold 4 decreases upwards, from 103 m at H7 to 58 m at H8 (Figs 3 and 8). Relative to regional stratal thickness patterns, we observe minor variations in H2–H8 thickness across folds 1-3, whereas a prominent thinning is observed across Fold 4 (Fig. 9). The base of S1-S4 are currently located ~1.58 km, ~1.58 km, ~1.53 km, and ~1.55 km beneath H8, respectively.

Figure 9: Thickness (Thick.) maps for intervals H2–H8, H8–H9, and H9–H10.

4.2.2 Fold geometries between H8–H10

Within Fold 1 and between H8–H10 (i.e. the fold top), we observe numerous seismic stratigraphic onlap and truncation relationships at various structural levels, particularly onto H8, H9, and H10 (Fig. 6). The base of S1 is currently located ~1.95 km beneath H10. From H8 to H10, there is a gradual transition in the morphology of Fold 1 from flat-topped to dome-shaped, which corresponds to an increase in fold amplitude from 59 m at H8, to 120 m at H9, and 90 m at H10 (Figs 3B, 6, and 8). This change in Fold 1 morphology occurs between H8–H9, where the thickness of this stratal package increases from ~230 m beyond the immediate fold periphery up to ~303 m across the fold crest (Fig. 9). There are several reflections between H8–H9, which apparently downlap onto underlying reflections and only occur within the limits of Fold 1 (Fig. 6).

Fold 2 displays onlap and truncation patterns from just below H8 to H10, where it has a maximum amplitude of 64 m, but its geometry remains flat-topped and the H8–H10 strata thin across the fold (Figs 7A, 8, and 9). The base of S2 is currently located ~1.83 km beneath H10. Onlap and truncation patterns are also observed in Fold 3 between H7 and H9 (i.e. the top of the fold), where it has an amplitude of 125 m (Fig. 7B). The base of S3 is currently located ~1.61 km beneath H9. We only observe onlap onto the top of Fold 4 at H8 (Fig. 3B). Folds 1-3 are, in places, incised by presumably deep-marine channels (e.g., Figs 3 and 7B).

4.3 Mound-like structures

Associated with folds 1 and 2 are a series of craters, dome-, and eye-shaped mounds that truncate and/or downlap onto various stratigraphic horizons between H8–H10, and are onlapped by overlying strata (e.g., Figs 7A and 10). These mounds have diameters and heights of ~200–500 m and ~30–80 m, respectively (e.g., Figs 7A and 10). All mounds are located at the fold peripheries and underlain by a zone of low-amplitude, chaotic reflections that extends down to lateral sill terminations (e.g., Fig. 10).

Figure 10: (A) Root mean squared (RMS) amplitude map of H8 over S1. Warm colours correspond to areas of high amplitude, whereas cold colours are areas of low amplitude. Hydrothermal vent conduits are highlighted by the red circles. (B) Interpreted

seismic section showing a hydrothermal vent, onlapped by overlying strata, and underlain by a pipe-like zone of disturbed reflections. See Figure 10A for location.

5 DISCUSSION

5

5.1 Magma emplacement

Space to accommodate magma intrusion is commonly generated by deformation of the host rock. At shallow-levels in sedimentary basins, intrusions often develop sill-like geometries as magma is emplaced along mechanical contrasts between layered strata, weak sedimentary rocks, and/or the minimum principal stress axis rotates to vertical (e.g., Kavanagh et al., 2006; Gudmundsson, 2011; Schofield et al., 2012; Magee et al., 2016; Walker et al., 2017). As intrusion continues and the sill inflates, space can be generated by uplift of the overburden and free surface to form dome-shaped forced folds (e.g., Pollard and Johnson, 1973; Hansen and Cartwright, 2006). Ground deformation driven by intrusion-induced forced folding is akin to the uplift observed at active volcanoes generated by magma movement and accumulation (e.g., Castro et al., 2016; Magee et al., 2017a). Given the broad spatial coincidence between fold outlines and sill terminations (e.g., Figs 3 and 5-7), we suggest that folds 1-3 formed in response to the intrusion of S1-S3, respectively (Stearns, 1978; Hansen and Cartwright, 2006). This forced fold interpretation is supported by evidence of onlap onto folds 1-3 at various stratigraphic levels (Figs 3, 6, and 7), which indicates that the domes had a bathymetric expression (e.g., Trude et al., 2003; Hansen and Cartwright, 2006). S4 is broadly overlain by a dome-shaped fold, which is onlapped at H8 by overlying strata, but the fold extends beyond the limit of the sill to the SE by up to ~6 km (Fig. 5). We suggest that part of Fold 4 was generated in response to sill emplacement but has interfered and merged with a differential compaction fold developed over the NE-SW oriented basement high (Figs 3, 5, and 8).

5.1.1 Timing of sill construction

Identification of onlapping reflections onto numerous stratigraphic horizons between H8–H10 and H7–H9 within folds 1-2 and Fold 3, respectively, indicate that sill emplacement instigated doming of the palaeo-seabed for a prolonged period of time (Figs 3, 6, and 7). Similarly, the mound-like structures, which are reminiscent of and interpreted to be hydrothermal vents, occur at various stratigraphic levels between H8–H10 and are onlapped by overlying strata (e.g., Fig. 10) (e.g., Jamtveit et al., 2004; Hansen, 2006). We recognise four main phases of intrusion, based on prominent seismic-stratigraphic onlap and truncation relationships at H7 for Fold 3, H8 for folds 1-4, H9 for folds 1 and 3, and H10 for folds 1 and 2 (Figs 3, 6, and 7). Biostratigraphic dating of these sedimentary horizons within the interval of interest indicates that sill emplacement principally occurred in the Oligocene (i.e. H7–H8, ~35–32 Ma), the Early Miocene (i.e. H9, ~19–16 Ma), and the Early Pliocene (i.e. H10, ~5–4 Ma) (Fig. 2). The occurrence of subtle onlap and truncation observed within folded strata deposited between these

principal phases of magmatism implies that sill emplacement occurred intermittently over ~31 Myr (Figs 3, 6, and 7), consistent with previous observations that sills and sill-complexes can assemble incrementally via the accumulation of relatively small-volume magma pulses intruded across protracted periods of time (e.g., Annen, 2011; Magee et al., 2014; Annen et al., 2015; Magee et al., 2016; Magee et al., 2017a). We cannot constrain the precise volumes and timing of individual sill emplacement events because: (i) we cannot seismically image presumably thin sills fed by discrete magma pulses; and (ii) we lack detailed biostratigraphic data to constrain the precise ages of the key onlap surfaces and strata deposited during periods of forced folding.

Given that S1-S4 are elongated ~E-W (Fig. 5), we consider it plausible that magma ascent (e.g., via dykes) and emplacement was influenced by the E-W striking Cretaceous normal faults that formed the Canterbury Basin and dissect the basement (Ghisetti and Sibson, 2012); basement-involved normal faults have also been shown to effect magma input and sill geometry in the Faroe-Shetland Basin, NE Atlantic (Schofield et al., 2017). Initial formation of S1-S4 likely occurred in the Katiki or Moreaki formations at structural levels, where host rock properties or stress conditions favoured sill emplacement (e.g., Kavanagh et al., 2006; Gudmundsson, 2011; Schofield et al., 2012), and were at least partly accommodated by forced folding (e.g., Figs 2 and 3). We suggest that later magma pulses utilised previous pathways into the basin (e.g., dykes) and became trapped by pre-existing components of S1-S3, where the new pulses promoted further sill construction and were accommodated by the reactivated growth of the forced folds. The trapping mechanism of later pulses will have principally been controlled by the relative timing of the different magma pulses and the thermal history of the intrusions and host rock (e.g., Annen, 2011; Annen et al., 2015; Magee et al., 2016). For example, if there is sufficient time for previous magma pulses to fully crystallise, their basal contact with the underlying sedimentary host rock will act as a rigidity barrier that can deflect and trap intruding magma along its surface (e.g. Kavanagh et al., 2006; Annen, 2011; Annen et al., 2015). Alternatively, if the time interval between emplaced magma pulses is short and/or earlier intrusions have thermally equilibrated with the host rock (i.e. they are crystalline mushes that retain residual melt), new magma injections may rejuvenate and mix with the partly solidified, pre-existing sill(s) (Annen, 2011). Whilst unravelling sill construction is critical to assessing their structural and thermal evolution, as well as that of the host rock, the limited spatial and temporal resolution of seismic reflection data means these hypotheses cannot be tested without additional information (e.g., biostratigraphic data from boreholes) or improvements in seismic imaging. However, because our observations indicate emplacement of S1-S4 occurred over 31 Myr at relatively shallow levels, probably <2.5 km considering current basal sill depths beneath H8–H10 are <2 km and typically ~1.6 km, we consider it most likely that the low temperature host rock would have promoted full solidification of magma pulses before later magma pulses intruded.

5.1.2 Fold amplitude as a proxy for sill thickness

Assuming that shallow-level sill emplacement is fully accommodated by elastic bending of the overburden implies that the amplitude of a forced fold is equivalent to the thickness of the forcing intrusion (Fig. 11A) (e.g., Pollard and Johnson, 1973;

Gouly and Schofield, 2008; Jackson et al., 2013). Inversion of ground deformation data collected from active volcanoes and related to subsurface magma movement also typically assumes that host rock deformation occurs via elastic bending, such that the size and location of the surface uplift and/or subsidence is expected to broadly reflect the volume and position of the magma body (e.g., Biggs et al., 2011; Galland, 2012; Pagli et al., 2012). If space for magma emplacement is also generated by the contemporaneous occurrence of inelastic host rock deformation processes (e.g., fluidisation and porosity reduction), fold amplitude will be less than the thickness of the intrusion (e.g., Jackson et al., 2013; Magee et al., 2013; Magee et al., 2017b).

Figure 11: (A) Schematic summarising the expected fold geometry and onlap relationships for forced folds, specifically folds 1 and 3. (B) Schematic describing how evacuation of a tabular sill and formation of inclined limbs can drive subsidence across the crest of a forced fold, which can accommodate depositing sediments. Repeated sill inflation/deflation and forced fold uplift/subsidence cycles could produce the observed upward increase in fold amplitude from H8 to H9 and thickening of the H8–H9 strata across the fold. (C) Schematic showing how the occurrence of seismically undetected, thin sills within the fold could produce the observed upward increase in fold amplitude from H8 to H9 and thickening of the H8–H9 strata across the fold. All figure parts are drawn to the same relative scale, such that differences in deformation style between the models can be compared. Also note that although the schematics only depict one sill, which grows through injection of new magma, it is plausible that the actual imaged intrusions consist of multiple accreted sills (e.g., Annen, 2011).

The sills imaged in seismic reflection data here are expressed as tuned reflection packages and are therefore probably <56 m thick, assuming the intrusions have an average interval velocity of 5550 m s⁻¹. However, all maximum fold amplitudes measured at identified fold tops are ≥59 m and up to 125 m (i.e. Fold 3 at H9); if sill thickness is at the limit of detectability (i.e. 7 m), differences between fold amplitude and sill thickness could thus be up to ~120 m. Furthermore, because the folded sedimentary succession has been compacted during burial, the measured fold amplitudes and, thus, the discrepancies between sill thickness and fold amplitude are minimum estimates. These unexpected discrepancies where fold amplitude is greater than sill thickness could be because: (i) the sills have a faster average interval velocity than 5550 m s⁻¹, which would increase the limit of separability (e.g., an interval velocity of ≥5900 m s⁻¹ would mean the sills could be ≥59 m thick; Fig. 12); (ii) the seismic velocity of the sedimentary sequence is overestimated, meaning that depth-converted fold amplitudes are accentuated, although we note that the increased depth of the study area relative to the boreholes implies the velocities used are minimum end-members; and/or (iii) multiple, seismically undetectable sills (i.e. <7 m thick) contributed to fold generation.

Figure 12: Graph showing the limits of separability and detectability for the seismic data, which has a frequency of ~25 Hz, if velocity of the igneous intrusions range from 4000–7500 m s⁻¹ (Magee et al., 2015). The minimum fold amplitude measured (i.e. 59 m) is shown, revealing that intrusion velocities of ≥5900 m s⁻¹ are required for sill thickness to equal measured fold amplitudes (grey).

In addition to the discrepancy between maximum forced fold amplitude and sill thickness, our observations reveal that amplitude varies with stratigraphic level. For example, Fold 4 has an amplitude of 103 m at H7 but 58 m at H8 (i.e. the top of the fold) (Fig. 3B). Because Fold 4 is only overlapped at H8 (Fig. 3B), suggesting it formed in a single intrusion event, the upwards decay in fold amplitude may relate to a syn-kinematic increase in ductile strain and inelastic deformation (e.g., compaction) towards the top of the fold (e.g., Pollard and Johnson, 1973; Hansen and Cartwright, 2006). Fold 2 also decreases in amplitude upwards, from 78 m at H8 to 64 m at H10 (Figs 7A and 8), but developed across multiple intrusion events. The upper portions of Fold 2, between H8–H10 are thus expected to have been superimposed and added onto the original forced fold generated in the Oligocene. For Fold 2, the formation of a 64 m high fold during the Early Pliocene implies that the Oligocene fold had an original amplitude of 14 m.

10

In contrast to folds 2 and 4, the amplitude of folds 1 and 3 increases with stratigraphic height; i.e. Fold 1 increases in amplitude from 59 m at H8 to 120 m at H9, decreasing to 90 m at H10, whereas Fold 3 has an amplitude of 110 m at H8 but 125 m at H9 (Figs 6, 7B, and 8). These increases in amplitude are associated with a change in fold geometry from flat-topped to dome-shaped and a subtle increase thickness of the H8–H9 sequence across folds 1 and 3 (Figs 6, 7B, 8, and 9). Within Fold 1, where the change in fold style from H8 to H9 is more prominent, the increased amount of reflections within the fold and presence of seismic-stratigraphic onlap and apparent downlap (i.e. rotated onlaps) suggest that there are several, thin packages of material that only occur across the fold crest (Fig. 6). These additional rock packages, which are restricted to the fold, accommodate the observed increase in amplitude and H8–H9 thickness (Fig. 6). It is important to note that these increases in amplitude and thickness, a change in fold morphology (i.e. from flat-topped to dome-shaped), and occurrence of additional material solely within the folded sequence contrasts with our conceptual model of intrusion-induced forced folding (Fig. 11A) (cf. Pollard and Johnson, 1973; Hansen and Cartwright, 2006; Galland, 2012; Magee et al., 2014). For example, because the geometry and growth of forced folds are controlled by a directly underlying forcing member, it is expected that whatever happens to the upper layers within a forced fold must also happen to the lower layers (Fig. 11A) (Stearns, 1978).

25

We suggest that the protracted development of Fold 1, and to a lesser extent Fold 3, involved repeated episodes of uplift and subsidence related to several discrete periods of sill injection and evacuation (Fig. 11B). In particular, we envisage that the intrusion and inflation of tabular sills uplifted the overburden to form flat-topped folds, which were expressed at the palaeosurface (Fig. 11B; Time 1). It is likely that Fold 1 formation was facilitated by circumferential reverse faulting and elastic bending (Figs 5, 6, and 11). Whilst many previous seismic-based studies have not recognised reverse faults associated with forced folding (e.g., Trude et al., 2003; Hansen et al., 2008; Jackson et al., 2013; Magee et al., 2013), analogue modelling experiments show that reverse faults can accompany forced fold formation (e.g., Galetto et al., 2017; Montanari et al., 2017). With inflation and bending of the overburden, eventual tensile fracturing of the host rock immediately overlying the lateral terminations of the tabular sill allows magma to transgress upwards and form the inclined limbs of a widening saucer-shaped sill (Fig. 11B; Time 1). Exploitation of reverse faults by magma may also promote inclined limb development (Figs 6 and 11).

30

If the melt supply to the entire sill wanes during the emplacement of the inclined limbs, their propagation could be further driven by magma evacuating from the inner, tabular sill in response to roof subsidence; i.e. magma pressure decreases below the lithostatic load, promoting relaxation (subsidence) of the elastically bended strata and compression of the inner sill (Fig. 11B; Time 2). Such a redistribution of magma would maintain or enhance the original flat-topped fold around its rim but promote subsidence of the fold crest, which may be infilled by depositing sediment, as the underlying inner sill thins (Fig. 11B; Time 2). Where a later injection of magma into the inner sill or along its contact re-inflates the forced fold, the strata deposited within the folded sequence will rotate and appear to downlap onto the underlying surface, producing a more dome-shaped fold geometry (Fig. 11B; Time 4). The seismic imaging of these stratal packages restricted to the folded sequence implies that there was time between intrusion events for a sufficiently thick sedimentary succession to be deposited (e.g., Fig. 11B). Unfortunately, we lack the high-resolution lithological and biostratigraphic data required to determine the sedimentation rate of these fold-restricted strata and, thereby, cannot constrain the time between distinct periods of sill emplacement. Overall, repeated periods of sill injection and evacuation into the inclined limbs over a protracted period of time could explain the observed increase in fold amplitude and stratal thickness, as well as the occurrence of fold-restricted reflections, as observed in folds 1 and 3 between H8–H9 (Figs 6, 7B, 8, 9, and 11B). Similar uplift and subsidence patterns have been observed to affect forced folds at active volcanoes, albeit on a much smaller spatial and temporal scale (Pagli et al., 2012; Magee et al., 2017a).

The injection of multiple, seismically undetectable, thin sills (i.e. <5 m thick) into the H8–H10 succession may also produce the observed fold geometries (Fig. 11C); this model could, to some extent, also explain the seismic-stratigraphic relationships if emplacement occurred incrementally. However, for Fold 1, a cumulative sill thickness of 59 m is required to increase the fold amplitude of 59 m at H8 to 120 m at H9. Whilst borehole from the Faroe-Shetland Basins suggest that a significant proportion of sills may not be resolved or detected in seismic reflection data (Schofield et al., 2017), perhaps supporting the thin sill model, a recent study has proposed that the high acoustic impedance contrast between igneous and sedimentary rocks means that even very thin sills should be detected in seismic data (Eide et al., 2017). We thus consider it unlikely that multiple, thin sills (<5 m thick) occur within the H8–H9 folded sequence of folds 1 and 3.

5.1.3 Tectono-magmatic context

Initial emplacement of S1–S3 during the Oligocene (35–32 Ma) was concurrent with emplacement of the Waiareka-Deborah volcanics and/or the Cookson volcanics (Fig. 2) (Timm et al., 2010). This magmatic event coincides with and may be genetically related to the opening and separation of Australia and Antarctica, which occurred ~33–30 Ma (e.g., Jenkins, 1974), and/or the northwards propagation of the Emerald Basin spreading zone (Uruski, 2010). Sill emplacement during the Early Miocene (~19–16 Ma) likely correlates to either the onshore development of the 27–12 Ma Oxford Volcanics in Central Canterbury or the 16–11 Ma Dunedin Volcano on the Otago Peninsula, which is located only ~50 km to the WSW of the study

area (Fig. 2). It is difficult to link Early Pliocene sill emplacement (5–4 Ma) to other magmatic events that occurred in and around the Canterbury Basin, although it may relate the ~2.6 Myr old basaltic Geraldine and Timaru lavas (Timm et al., 2010).

5.2 Implications for using seismic reflection data to inform interpretation of ground deformation at active volcanoes

5 Reflection seismology is the only technique that allows the entire 3D geometry of natural, shallow-level intrusions and associated host rock structures to be visualised and quantified at a relatively high-resolution (e.g., Smallwood and Maresh, 2002; Hansen and Cartwright, 2006; Magee et al., 2016). Seismic reflection data thus provides a unique opportunity to investigate how overburden uplift (i.e. forced folding) and subsidence accommodates intrusions and is expressed at the contemporaneous surface (e.g., Trude et al., 2003; Hansen and Cartwright, 2006; Jackson et al., 2013). For example, 10 discrepancies between fold amplitudes and intrusion thicknesses measured in seismic reflection data, coupled with field observations, have highlighted that inelastic deformation processes can play an important role in accommodating magma volumes (e.g., Jackson et al., 2013; Magee et al., 2013). To date, however, the vast majority of seismic-based studies examining intrusion-induced forced folds adopt an interpretation framework that assumes magma emplacement and fold growth occurred 15 instantaneously (e.g., Trude et al., 2003; Hansen and Cartwright, 2006; Jackson et al., 2013). Whilst this instantaneous model may be appropriate for forced folds developed during single, short-lived magma injection events, observations of active emplacement and host rock deformation from field-, geophysical-, and geodetic-based studies reveal that forced folds can evolve through multiple uplift and subsidence episodes (e.g., Sturkell et al., 2006; Magee et al., 2017a). It is thus difficult to reconcile insights into the processes controlling ground deformation obtained from seismic reflection data, which only provide 20 a snapshot of the cumulative strain accommodating ancient intrusions, and the dynamic uplift and subsidence recorded at active volcanoes. We show that mapping of intra-fold strata and identification of seismic-stratigraphic relationships can be used to unravel the incremental development of sill intrusions and overlying forced folds (see also Magee et al., 2014). Furthermore, our results provide the first evidence from seismic reflection data that the dynamic interplay between uplift and subsidence can control forced fold geometries. We suggest that broad areas of uplift likely correspond to the inflation of magma reservoirs, whereas the transition to broad subsidence and localised uplift (e.g., above inclined limbs of saucer-shaped sills) 25 marks the onset of magma transgression. Importantly, our observations also emphasise that relatively simple, transient uplift and subsidence patterns can be produced by complex intrusion morphologies (Galland, 2012; Magee et al., 2017a).

5.3 Implications for hydrocarbon exploration

Deciphering how the host rock deforms and accommodates the intruded magma volume is also important from a hydrocarbon 30 exploration perspective because: (i) elastic folding of the overburden and free surface above intruding, shallow-level (< 2 km depth) sills can produce forced folds that may result in the formation of structural (i.e. four-way dip closures) and stratigraphic (i.e. pinchout) traps (e.g., Reeckmann and Mebberson, 1984; Smallwood and Maresh, 2002; Schutter, 2003; Schmiedel et al.,

2017); (ii) intrusion-induced faulting and fracturing, which may accompany folding, can increase local permeability and potentially breach traps or compartmentalise reservoirs (e.g., Reeckmann and Mebberson, 1984; Holford et al., 2012; Holford et al., 2013); and (iii) inelastic deformation processes involving porosity reduction (e.g., compaction and fluidization) can inhibit hydrocarbon migration and reduce reservoir quality (Schofield et al., 2017). Sill emplacement in the petroliferous Canterbury Basin throughout the Oligocene-to-Early Pliocene overlapped with the onset of hydrocarbon generation and expulsion in the mid-Miocene (Fig. 2) (Bennett et al., 2000). The sills are spatially restricted and therefore likely to only influence any active petroleum system on a local scale. Sills intrude Cretaceous-to-Palaeogene strata, where the principal source rocks (e.g., coals) are expected (Figs 2, 3, and 6). The imaged sills are probably <55m thick but their impact on source rock maturity is unknown; e.g., sill intrusion could mature or overmature any surrounding source rocks (e.g., Rodriguez Monreal et al., 2009; Holford et al., 2013). Furthermore, it is probable that igneous bodies below the resolution of the seismic data are present and could impact maturation dynamics (Schofield et al., 2017). The forced folds deform potential Late Cretaceous and Eocene reservoir rocks, creating possible structural traps (Figs 2, 3, and 6). Other potential traps associated with the forced folds are created by the onlap of strata onto the domes (Fig. 6) (Smallwood and Maresh, 2002; Magee et al., 2017b). Overall, whilst it is difficult to assess whether sill emplacement had a beneficial or adverse effect on petroleum system development, our study highlights that it is critical to not only elucidate magma emplacement mechanics, but also to determine the timing of magmatism relative to hydrocarbon generation and migration.

6 CONCLUSIONS

20 Emplacement of shallow-level sills in sedimentary basins is commonly accommodated by overburden uplift to produce a forced fold that is expressed at the contemporaneous surface. The geometry and kinematics of these intrusion-induced forced folds reflects sill emplacement processes and thus sheds light on how ground deformation relates to magma movement at active volcanoes. Here, we use 3D seismic reflection data from the Canterbury Basin, offshore SE New Zealand, to analyse the timing and formation of four saucer-shaped sill and forced fold pairs. Seismic-stratigraphic onlap and truncation relationships reveal that sill emplacement initially occurred in the Oligocene (~35–22 Ma), followed by two other major intrusive phases in the Early Miocene (~19–16 Ma) and Early Pliocene (~5–4 Ma); these observations indicate that we should not rely on simply identifying onlap relationships at the top of forced folds to assess the age of sill emplacement. Evidence of forced fold growth between these main magmatic events indicates that sill emplacement occurred incrementally over a protracted timespan (~31 Myr). Whilst two of the forced folds conform to the traditional conceptual models of forced fold growth, i.e. fold amplitude decreases up and away from the underlying forcing body, two folds exhibit an upward increase in fold amplitude and a change in morphology from flat-topped to dome-shaped. These changes in fold geometry correspond to the occurrence of additional seismic reflections across and restricted to the fold crests, which locally thicken the folded sequence. We suggest that this unexpected increase in fold amplitude and thickening of strata can be attributed to either: (i) repeated episodes of sill injection and inflation followed by magma evacuation into the inclined limbs of the saucer-shaped

sill, which promoted fold subsidence and locally accommodated deposition of sediments restricted to the deformed sequence; or (ii) the emplacement of seismically undetectable, thin sills within the folded sequence. Furthermore, by unravelling forced fold kinematics, we demonstrate that sill emplacement spanned the generation, migration, and accumulation of hydrocarbons, potentially influencing local petroleum system development. Our observations show that changes in ground deformation patterns, specifically the localisation of uplift and onset of broad subsidence, may indicate magma transgression. Overall, our study shows that analysing structural and stratigraphic relationships across the entire height of a forced fold can provide critical insight into the long-term and dynamic evolution of sill emplacement and associated ground deformation.

AUTHOR CONTRIBUTIONS

JR conducted the bulk of the seismic interpretation, analysis, and write-up as part of her MSci project at Imperial College London. CM designed the project, aided interpretation, and contributed significantly to the manuscript writing. CJ helped design the project, advised interpretations, and edited the manuscript.

ACKNOWLEDGEMENTS

CM is sponsored by an Imperial College Research Fellowship. We are grateful to New Zealand Petroleum and Minerals for data provision and Schlumberger for seismic interpretation software. We also thank numerous colleagues who attended the AAPG Geosciences Technology Workshop on ‘Influence of Volcanism and Associated Magmatic Processes on Petroleum Systems’ and John Cosgrove for their helpful insights into this work. We thank John Browning and Domenico Montanari for their constructive reviews and to Fabian Wadsworth for editorial handling.

DATA AVAILABILITY

All seismic and borehole data is freely available from New Zealand Petroleum and Minerals (<https://www.nzpam.govt.nz/>).

REFERENCES

- Annen, C. (2011). Implications of incremental emplacement of magma bodies for magma differentiation, thermal aureole dimensions and plutonism–volcanism relationships. *Tectonophysics*, 500(1), 3-10. <https://doi.org/10.1016/j.tecto.2009.04.010>
- Annen, C., Blundy, J. D., Leuthold, J., & Sparks, R. S. J. (2015). Construction and evolution of igneous bodies: Towards an integrated perspective of crustal magmatism. *Lithos*, 230, 206-221. <https://doi.org/10.1016/j.lithos.2015.05.008>
- Bennett, D., Brand, R., Francis, D., Langdale, S., Mills, C., Morris, B., & Tian, X. (2000). *Preliminary results of exploration in the onshore Canterbury Basin*. Paper presented at the 2000 New Zealand Petroleum Exploration Conference Proceedings.
- Biggs, J., Anthony, E., & Ebinger, C. (2009). Multiple inflation and deflation events at Kenyan volcanoes, East African Rift. *Geology*, 37(11), 979-982. <https://doi.org/10.1130/G30133A.1>

- Biggs, J., Bastow, I. D., Keir, D., & Lewi, E. (2011). Pulses of deformation reveal frequently recurring shallow magmatic activity beneath the Main Ethiopian Rift. *Geochemistry, Geophysics, Geosystems*, 12(9), Q0AB10. <http://dx.doi.org/doi:10.1029/2011GC003662>
- Brown, A. R. (2004). *Interpretation of three-dimensional seismic data* (6th ed. Vol. 42). Oklahoma, USA: AAPG and SEG.
- 5 Carter, R. (1988). Post-breakup stratigraphy of the Kaikoura Synthem (Cretaceous-Cenozoic), continental margin, southeastern New Zealand. *New Zealand journal of geology and geophysics*, 31(4), 405-429. <http://dx.doi.org/10.1080/00288306.1988.10422141>
- Castro, J. M., Cordonnier, B., Schipper, C. I., Tuffen, H., Baumann, T. S., & Feisel, Y. (2016). Rapid laccolith intrusion driven by explosive volcanic eruption. *Nature communications*, 7, 13585. <http://dx.doi.org/10.1038/ncomms13585>
- 10 Eide, C. H., Schofield, N., Lecomte, I., Buckley, S. J., & Howell, J. A. (2017). Seismic Interpretation of Sill-complexes in Sedimentary Basins: The 'sub-sill Imaging Problem'. *Journal of the Geological Society of London*
- Fulthorpe, C. S., Carter, R. M., Miller, K. G., & Wilson, J. (1996). Marshall Paraconformity: a mid-Oligocene record of inception of the Antarctic circumpolar current and coeval glacio-eustatic lowstand? *Marine and petroleum geology*, 13(1), 61-77. [https://doi.org/10.1016/0264-8172\(95\)00033-X](https://doi.org/10.1016/0264-8172(95)00033-X)
- 15 Galetto, F., Acocella, V., & Caricchi, L. (2017). Caldera resurgence driven by magma viscosity contrasts. *Nature Communications*, 8(1), 1750. <https://doi.org/10.1038/s41467-017-01632-y>.
- Galland, O. (2012). Experimental modelling of ground deformation associated with shallow magma intrusions. *Earth and Planetary Science Letters*, 317, 145-156. <https://doi.org/10.1016/j.epsl.2011.10.017>
- Galland, O., & Scheibert, J. (2013). Analytical model of surface uplift above axisymmetric flat-lying magma intrusions: 20 Implications for sill emplacement and geodesy. *Journal of Volcanology and Geothermal Research*, 253, 114-130.
- Ghisetti, F. C. & Sibson, R. H. (2012). Compressional reactivation of E-W inherited normal faults in the area of the 2010–2011 Canterbury earthquake sequence. *New Zealand Journal of Geology and Geophysics*, 55(3), 177-184. <https://doi.org/10.1785/gssrl.82.6.824>
- Gouly, N. R., & Schofield, N. (2008). Implications of simple flexure theory for the formation of saucer-shaped sills. *Journal of Structural Geology*, 30(7), 812-817. <https://doi.org/10.1016/j.jvolgeores.2012.12.006>
- 25 Gudmundsson, A. (2011). Deflection of dykes into sills at discontinuities and magma-chamber formation. *Tectonophysics*, 500(1-4), 50-64. <https://doi.org/10.1016/j.tecto.2009.10.015>
- Hansen, D. M. (2006). The morphology of intrusion-related vent structures and their implications for constraining the timing of intrusive events along the NE Atlantic margin. *Journal of the Geological Society of London*, 163, 789-800. <https://doi.org/10.1144/0016-76492004-167>
- 30 Hansen, D. M., & Cartwright, J. (2006). The three-dimensional geometry and growth of forced folds above saucer-shaped igneous sills. *Journal of Structural Geology*, 28(8), 1520-1535. <https://doi.org/10.1016/j.jsg.2006.04.004>

- Hansen, D. M., Redfern, J., Federici, F., Di Biase, D., & Bertozzi, G. (2008). Miocene igneous activity in the Northern Subbasin, offshore Senegal, NW Africa. *Marine and Petroleum Geology*, 25(1), 1-15. <https://doi.org/10.1016/j.marpetgeo.2007.04.007>
- 5 Holford, S. P., Schofield, N., MacDonald, J. D., Duddy, I. R., & Green, P. F. (2012). Seismic analysis of igneous systems in sedimentary basins and their impacts on hydrocarbon prospectivity: examples from the southern Australian margin. *APPEA Journal*, 52, 23. <https://doi.org/10.1071/AJ11017>
- Holford, S. P., Schofield, N., Jackson, C. A. L., Magee, C., Green, P. F., & Duddy, I. R. (2013). Impacts of igneous intrusions on source and reservoir potential in prospective sedimentary basins along the western Australian continental margin. In M. Keep & S. J. Moss (Eds.), *The Sedimentary Basins of Western Australia IV*. Perth, WA: Proceedings of the Petroleum Exploration Society of Australia Symposium.
- 10 Jackson, C. A.-L., Schofield, N., & Golenkov, B. (2013). Geometry and controls on the development of igneous sill-related forced folds: A 2-D seismic reflection case study from offshore southern Australia. *Geological Society of America Bulletin*, 125(11-12), 1874-1890. <https://doi.org/10.1130/B30833.1>
- Jamtveit, B., Svensen, H., Podladchikov, Y. Y., & Planke, S. (2004). Hydrothermal vent complexes associated with sill intrusions in sedimentary basins. *Physical geology of high-level magmatic systems*, 234, 233-241.
- 15 Jenkins, D. G. (1974). Initiation of the proto circum-Antarctic current. *Nature*, 252(5482), 371-373. <https://doi.org/10.1038/252371a0>
- Johnson, D. J. (1987). Elastic and inelastic magma storage at Kilauea volcano. *US Geological Survey Professional Paper*, 1350, 1297-1306.
- 20 Kavanagh, J. L., Menand, T., & Sparks, R. S. J. (2006). An experimental investigation of sill formation and propagation in layered elastic media. *Earth and Planetary Science Letters*, 245(3-4), 799-813. <https://doi.org/10.1016/j.epsl.2006.03.025>
- Killops, S., Cook, R., Sykes, R., & Boudou, J. (1997). Petroleum potential and oil-source correlation in the Great South and Canterbury Basins. *New Zealand journal of geology and geophysics*, 40(4), 405-423. <http://dx.doi.org/10.1080/00288306.1997.9514773>
- 25 Lu, H., & Fulthorpe, C. S. (2004). Controls on sequence stratigraphy of a middle Miocene–Holocene, current-swept, passive margin: Offshore Canterbury Basin, New Zealand. *Geological Society of America Bulletin*, 116(11-12), 1345-1366. <https://doi.org/10.1130/B2525401.1>
- Lu, H., Fulthorpe, C. S., Mann, P., & Kominz, M. A. (2005). Miocene–Recent tectonic and climatic controls on sediment supply and sequence stratigraphy: Canterbury basin, New Zealand. *Basin Research*, 17(2), 311-328. <http://dx.doi.org/10.1111/j.1365-2117.2005.00266.x>
- 30 Magee, C., Briggs, F., & Jackson, C. A.-L. (2013). Lithological controls on igneous intrusion-induced ground deformation. *Journal of the Geological Society of London*, 170(6), 853-856. <https://doi.org/10.1144/jgs2013-029>

- Magee, C., Jackson, C. L., & Schofield, N. (2014). Diachronous sub-volcanic intrusion along deep-water margins: insights from the Irish Rockall Basin. *Basin Research*, 26(1), 85-105. <http://dx.doi.org/10.1111/bre.12044>
- Magee, C., Maharaj, S. M., Wrona, T., & Jackson, C. A. L. (2015). Controls on the expression of igneous intrusions in seismic reflection data. *Geosphere*, 11(4), pp.1024-1041. <https://doi.org/10.1130/GES01150.1>
- 5 Magee, C., Muirhead, J. D., Karvelas, A., Holford, S. P., Jackson, C. A., Bastow, I. D., . . . McCarthy, W. (2016). Lateral magma flow in mafic sill complexes. *Geosphere*, GES01256. 01251. <https://doi.org/10.1130/GES01256.1>
- Magee, C., Bastow, I. D., de Vries, B. v. W., Jackson, C. A.-L., Hetherington, R., Hagos, M., & Hoggett, M. (2017a). Structure and dynamics of surface uplift induced by incremental sill emplacement. *Geology*, 45(5), 431-434. <https://doi.org/10.1130/G38839.1>
- 10 Magee, C., Jackson, C. A.-L., Hardman, J. P., & Reeve, M. T. (2017b). Decoding sill emplacement and forced fold growth in the Exmouth Sub-basin, offshore northwest Australia: Implications for hydrocarbon exploration. *Interpretation*, 5(3), SK11-SK22. <https://doi.org/10.1190/INT-2016-0133.1>
- Monatanri, D., Bonini, M., Corti, G., Agostini, A., & Del Ventisette, C. (2017). Forced folding above shallow magma intrusions: Insights on supercritical fluid flow from analogue modelling. *Journal of Volcanology and Geothermal Research*, 245, 67-80. <https://doi.org/10.1016/j.jvolgeores.2017.07.022>
- 15 Pagli, C., Wright, T. J., Ebinger, C. J., Yun, S.-H., Cann, J. R., Barnie, T., & Ayele, A. (2012). Shallow axial magma chamber at the slow-spreading Erta Ale Ridge. *Nature Geoscience*, 5(4), 284-288. <https://doi.org/10.1038/ngeo1414>
- Pollard, D. D., & Johnson, A. M. (1973). Mechanics of growth of some laccolithic intrusions in the Henry Mountains, Utah, II: bending and failure of overburden layers and sill formation. *Tectonophysics*, 18(3), 311-354. [https://doi.org/10.1016/0040-1951\(73\)90051-6](https://doi.org/10.1016/0040-1951(73)90051-6)
- 20 Reeckmann, S. A., & Mebberson, A. J. (1984). Igneous intrusions in the North-West Canning Basin and their impact on oil exploration. In P. G. Purcell (Ed.), *The Canning Basin, WA* (pp. 389-399). Perth, WA: Proceedings of the Geological Society of Australia/Petroleum Exploration Society of Australia Canning Basin Symposium.
- Rodriguez Monreal, F., Villar, H., Baudino, R., Delpino, D., & Zencich, S. (2009). Modeling an atypical petroleum system: a case study of hydrocarbon generation, migration and accumulation related to igneous intrusions in the Neuquen Basin, Argentina. *Marine and petroleum geology*, 26(4), 590-605. <https://doi.org/10.1016/j.marpetgeo.2009.01.005>
- 25 Schmiedel, T., Kjoberg, S., Planke, S., Magee, C., Galland, O., Schofield, N., . . . Jerram, D. A. (2017). Mechanisms of overburden deformation associated with the emplacement of the Tulipan sill, mid-Norwegian margin. *Interpretation*, 5(3), SK23-SK38. <https://doi.org/10.1190/INT-2016-0155.1>
- 30 Schofield, N. J., Brown, D. J., Magee, C., & Stevenson, C. T. (2012). Sill morphology and comparison of brittle and non-brittle emplacement mechanisms. *Journal of the Geological Society of London*, 169(2), 127-141. <https://doi.org/10.1144/0016-76492011-078>
- Schofield, N., Alsop, I., Warren, J., Underhill, J. R., Lehné, R., Beer, W., & Lukas, V. (2014). Mobilizing salt: Magma-salt interactions. *Geology*, G35406. 35401. <https://doi.org/10.1130/G35406.1>

- Schofield, N., Holford, S., Millett, J., Brown, D., Jolley, D., Passey, S. R., . . . Stevenson, C. (2017). Regional magma plumbing and emplacement mechanisms of the Faroe-Shetland Sill Complex: implications for magma transport and petroleum systems within sedimentary basins. *Basin Research*, 29(1), 41-63. <https://doi.org/10.1111/bre.12164>
- Schutter, S. R. (2003). Hydrocarbon occurrence and exploration in and around igneous rocks. *Geological Society, London, Special Publications*, 214(1), 7-33. <https://doi.org/10.1144/GSL.SP.2003.214.01.02>
- 5 Skogly, O. (1998). *Seismic characterization and emplacement of intrusives in the Vøring Basin*. (M.Sc. Thesis), University of Oslo.
- Smallwood, J. R., & Maresh, J. (2002). The properties, morphology and distribution of igneous sills: modelling, borehole data and 3D seismic from the Faroe-Shetland area. In D. W. Jolley & B. R. Bell (Eds.), *The North Atlantic Igneous Province: Stratigraphy, tectonic, Volcanic and Magmatic Processes* (Vol. 197, pp. 271-306): Geological Society, London, Special Publications. <https://doi.org/10.1144/GSL.SP.2002.197.01.11>
- 10 Sparks, R., Biggs, J., & Neuberg, J. (2012). Monitoring volcanoes. *Science*, 335(6074), 1310-1311. <https://doi.org/10.1126/science.1219485>
- Stearns, D. W. (1978). Faulting and forced folding in the Rocky Mountains foreland. *Geological Society of America Memoirs*, 151, 1-38. <https://doi.org/10.1130/MEM151-p1>
- 15 Sturkell, E., Einarsson, P., Sigmundsson, F., Geirsson, H., Ólafsson, H., Pedersen, R., . . . Stefánsson, R. (2006). Volcano geodesy and magma dynamics in Iceland. *Journal of Volcanology and Geothermal Research*, 150(1-3), 14-34. <https://doi.org/10.1016/j.jvolgeores.2005.07.010>
- Timm, C., Hoernle, K., Werner, R., Hauff, F., van den Bogaard, P., White, J., . . . Garbe-Schönberg, D. (2010). Temporal and geochemical evolution of the Cenozoic intraplate volcanism of Zealandia. *Earth-Science Reviews*, 98(1), 38-64. <https://doi.org/10.1016/j.earscirev.2009.10.002>
- 20 Trude, J., Cartwright, J., Davies, R. J., & Smallwood, J. R. (2003). New technique for dating igneous sills. *Geology*, 31, 4. <https://doi.org/10.1130/G19559.1>
- Uruski, C. I. (2010). New Zealand's deepwater frontier. *Marine and petroleum geology*, 27(9), 2005-2026. <https://doi.org/10.1016/j.marpetgeo.2010.05.010>
- 25 van Wyk de Vries, B., Márquez, A., Herrera, R., Bruña, J. G., Llanes, P., & Delcamp, A. (2014). Craters of elevation revisited: forced-folds, bulging and uplift of volcanoes. *Bulletin of Volcanology*, 76(11), 1-20. <https://doi.org/10.1007/s00445-014-0875-x>
- Walker, R., Healy, D., Kawanzaruwa, T., Wright, K., England, R., McCaffrey, K., . . . Blenkinsop, T. (2017). Igneous sills as a record of horizontal shortening: The San Rafael subvolcanic field, Utah. *Geological Society of America Bulletin*, B31671. 31671. <https://doi.org/10.1130/B31671.1>
- 30

Figure 1

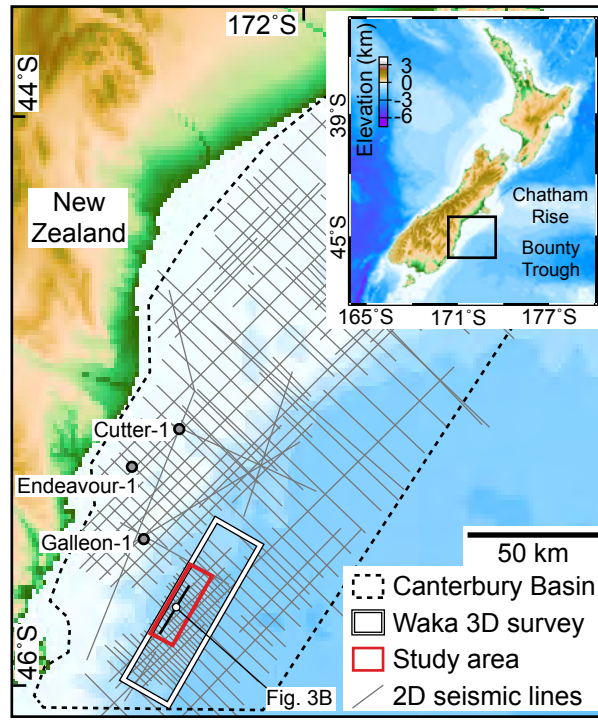


Figure 2

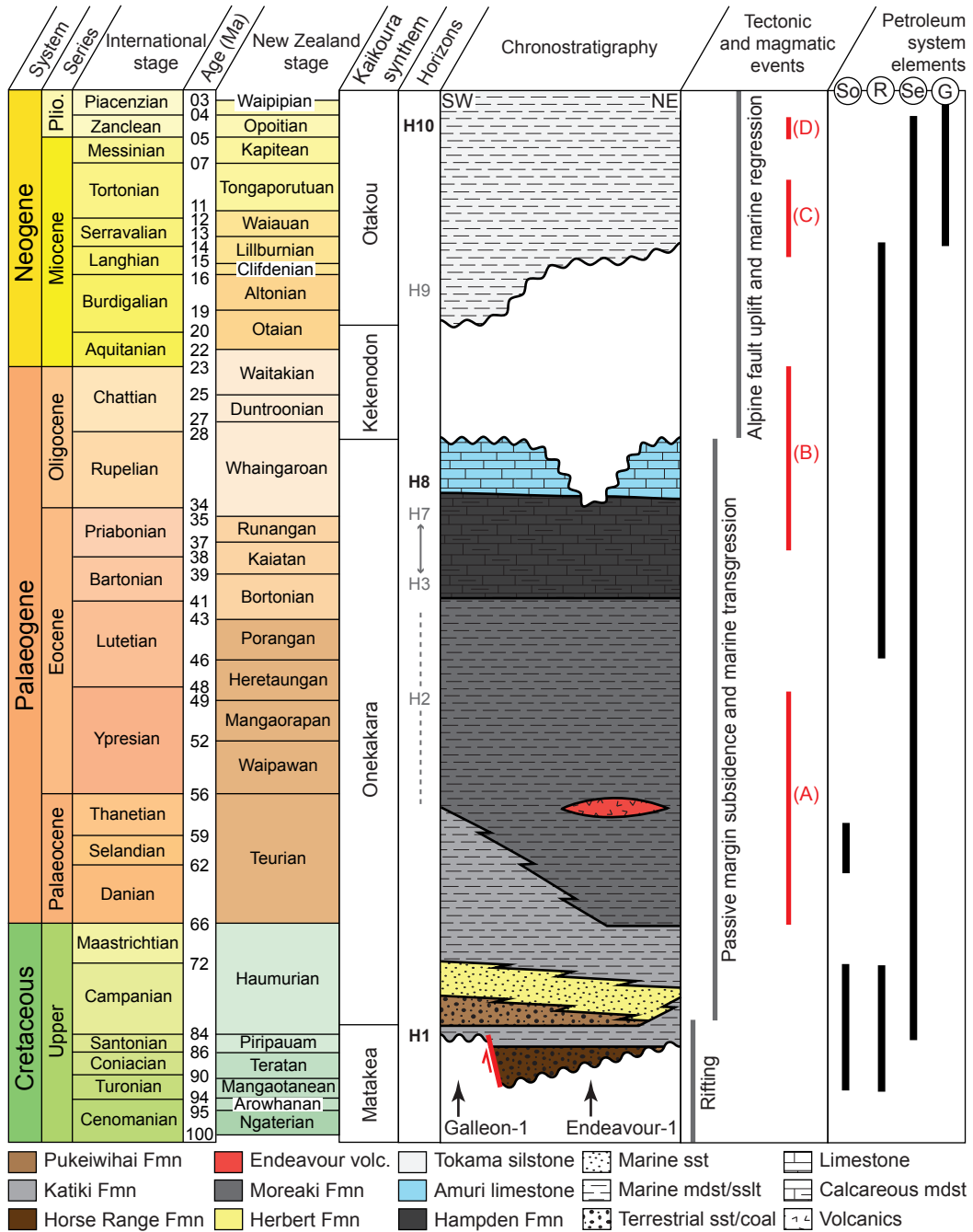


Figure 3

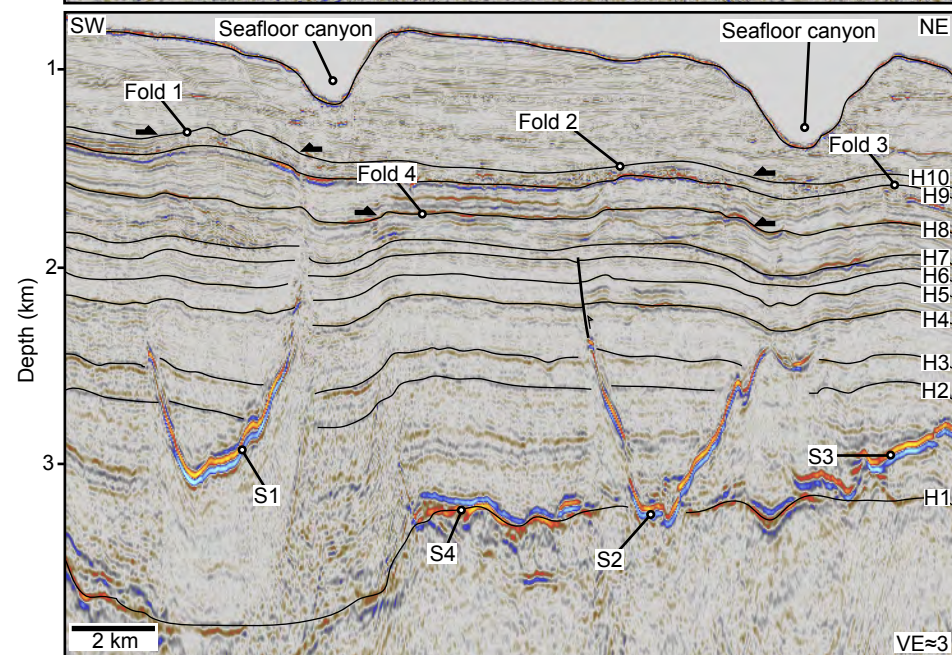
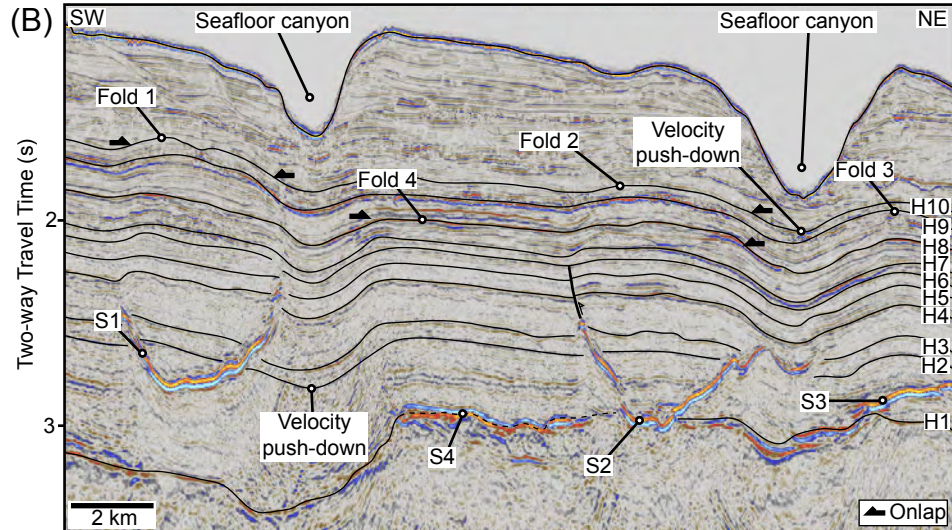
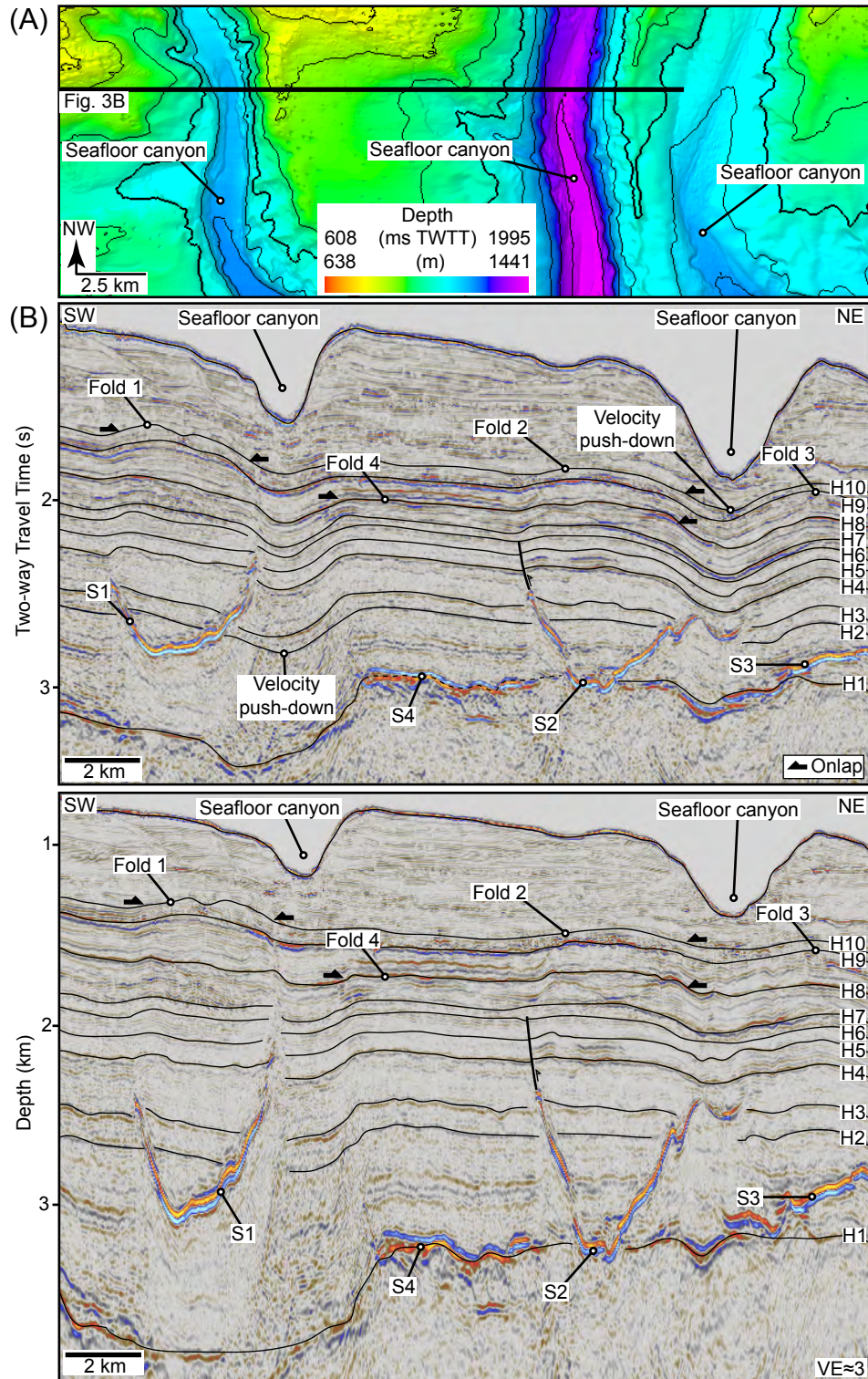


Figure 5

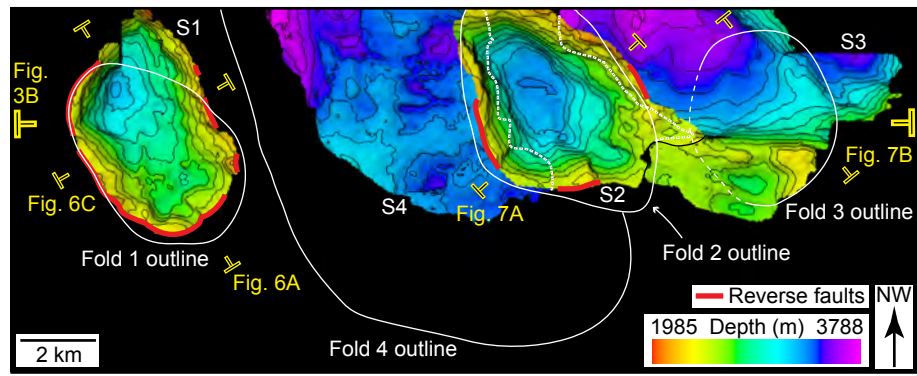


Figure 6

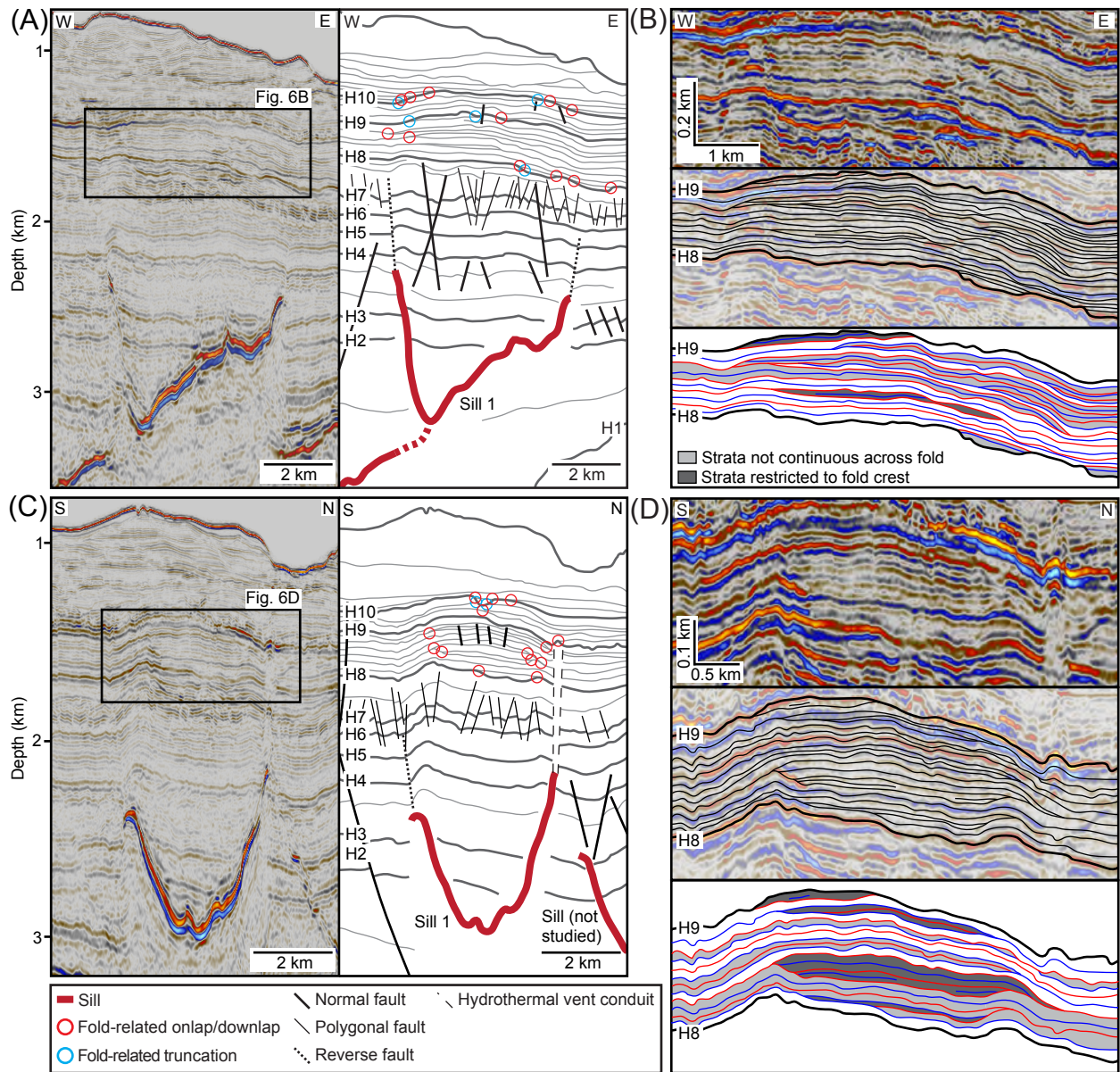


Figure 7

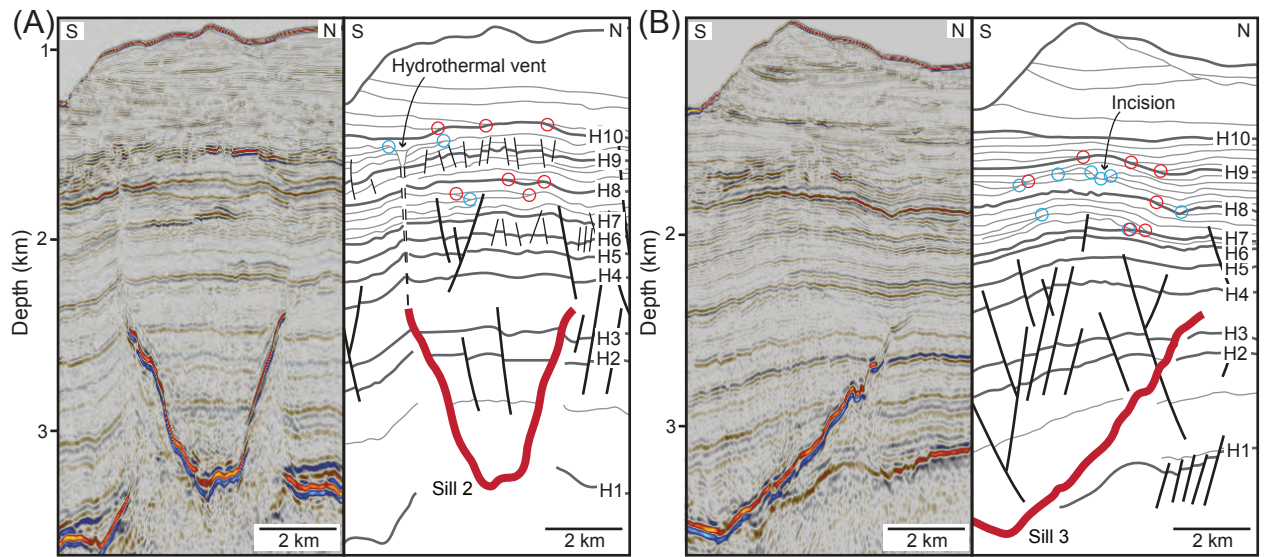


Figure 8

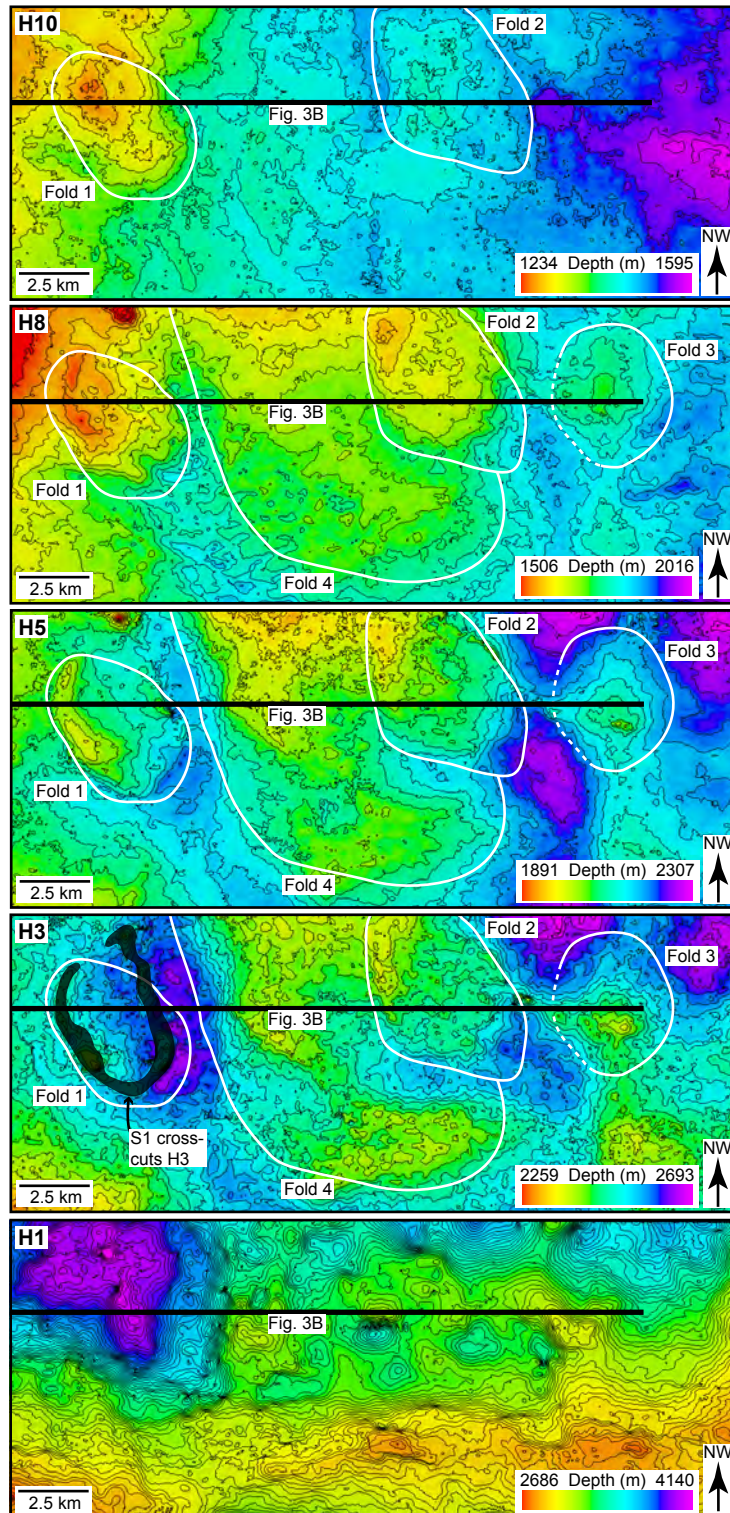


Figure 9

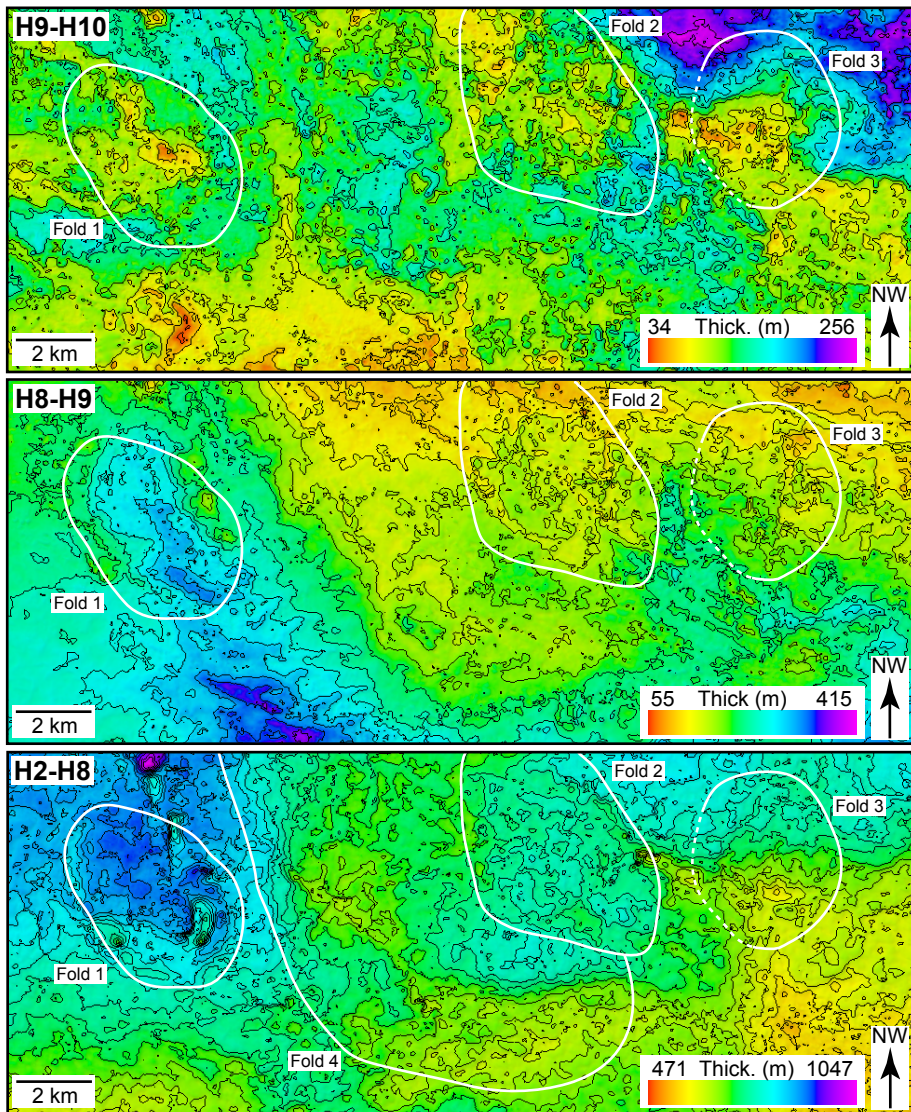


Figure 10

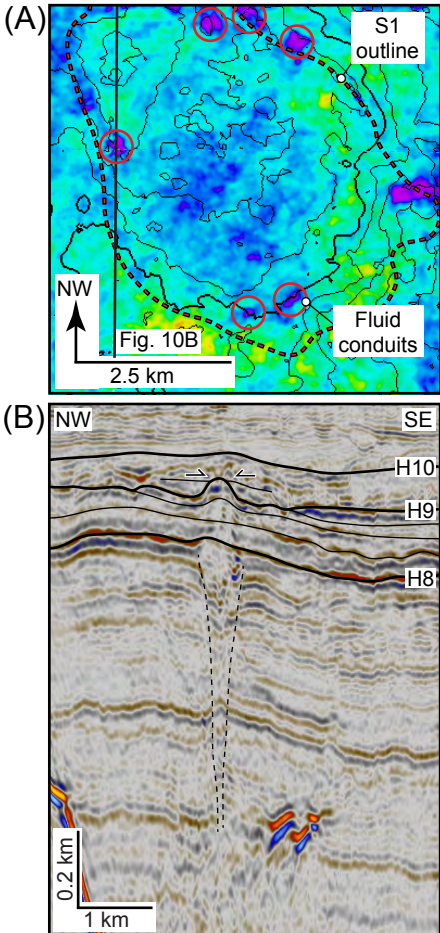


Figure 11

